Volume 7 | Number 19 | 7 October 2020

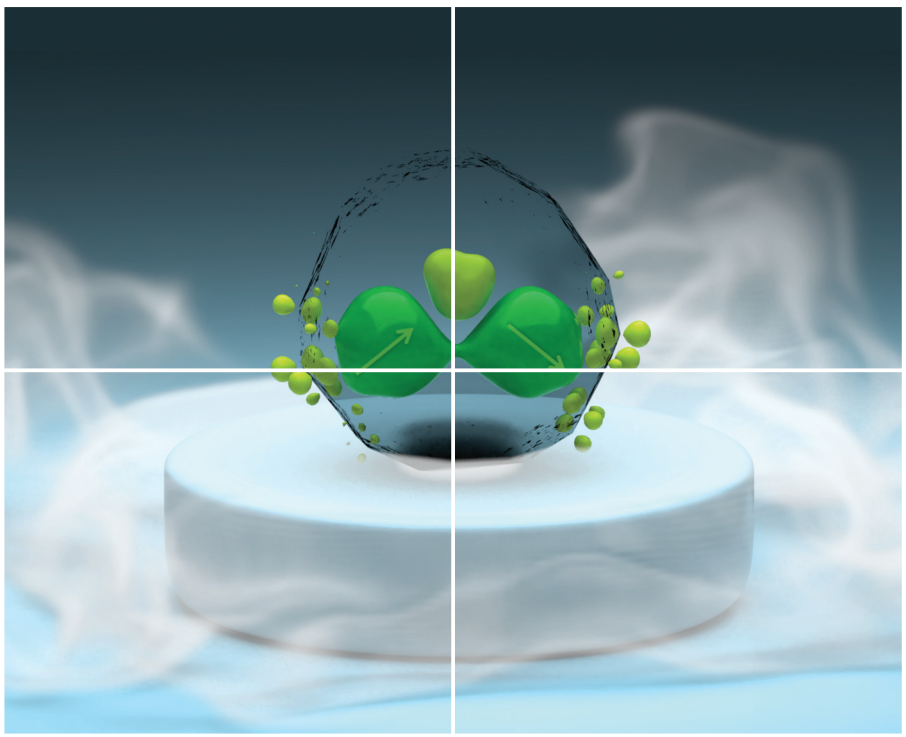

INORGANIC CHEMISTRY

FRONTIERS

CCS 中国化学会 CHINESE CHEMICAL SOCIETY

PEKING UNIVERSITY 1898

ROYAL SOCIETY OF CHEMISTRY

rsc.li/frontiers-inorganic

INORGANIC CHEMISTRY
FRONTIERS

RESEARCH ARTICLE

View Article Online
View Journal | View Issue

Cite this: *Inorg. Chem. Front.*, 2020, **7**, 3521

Magnetic hysteresis and strong ferromagnetic coupling of sulfur-bridged Dy ions in clusterfullerene $Dy_2S@C_{82}$†

Denis Krylov,[a,b] Georgios Velkos,[a] Chia-Hsiang Chen,[a,c] Bernd Büchner,[a] Aram Kostanyan,[d] Thomas Greber,[d] Stanislav M. Avdoshenko[a] and Alexey A. Popov*[a]

Received 29th June 2020,
Accepted 28th July 2020

DOI: 10.1039/d0qi00771d

rsc.li/frontiers-inorganic

Two isomers of metallofullerene $Dy_2S@C_{82}$ with sulfur-bridged Dy ions exhibit broad magnetic hysteresis with sharp steps at sub-Kelvin temperature. Analysis of the level crossing events for different orientations of a magnetic field showed that even in powder samples, the hysteresis steps caused by quantum tunneling of magnetization can provide precise information on the strength of intramolecular Dy···Dy interactions. A comparison of different methods to determine the energy difference between ferromagnetic and antiferromagnetic states showed that sub-Kelvin hysteresis gives the most robust and reliable values. The ground state in $Dy_2S@C_{82}$ has ferromagnetic coupling of Dy magnetic moments, whereas the state with antiferromagnetic coupling in C_s and C_{3v} cage isomers is 10.7 and 5.1 cm^{-1} higher, respectively. The value for the C_s isomer is among the highest found in metallofullerenes and is considerably larger than that reported in non-fullerene dinuclear molecular magnets. Magnetization relaxation times measured in zero magnetic field at sub-Kelvin temperatures tend to level off near 900 and 3200 s in C_s and C_{3v} isomers. These times correspond to the quantum tunneling relaxation mechanism, in which the whole magnetic moment of the $Dy_2S@C_{82}$ molecule flips at once as a single entity.

Introduction

Tremendous progress in lanthanide single-molecule magnets (SMMs) during the last decade had been largely fuelled by the design of new molecules with ever-increasing magnetic anisotropy.[1] For single-ion SMMs, ligand-field (LF) splitting has been the main parameter on which experimental and computational studies have focused until recently,[2] although the gradual understanding of the paramount role of molecular vibrations now shifts the focus to spin–phonon interactions.[2j,3] In polynuclear SMMs, exchange and dipolar interactions between lanthanide ions create a more complex structure of magnetic states than in single-ion magnets, and the presence of such coupled states introduces a strong variation in static and dynamic magnetic properties in comparison with their single-ion counterparts. The most obvious difference is the quenching of zero-field quantum tunneling of magnetization in dinuclear SMMs, which is caused by exchange biasing.[4] On the other hand, new relaxation pathways involving low-energy exchange-excited states can appear in dinuclear SMMs and limit their SMM performance.

Aside from compounds with lanthanide-radical coupling, which can be very strong,[5] magnetic Ln···Ln interactions are usually rather weak. The energy difference between the lowest states with ferromagnetically and antiferromagnetically coupled moments, ΔE_{AFM-FM}, is a very important parameter for dinuclear SMMs, but its precise determination is not very straightforward and often relies on the fitting of magnetic data with effective spin Hamiltonians involving some parameterized forms of Ln···Ln interactions. EPR studies can in principle provide more precise information on the Ln···Ln interactions,[6] but for lanthanide ions with strong magnetic anisotropy, such studies encounter serious difficulties and are still rare. At the same time, the orbital mechanisms behind the exchange interactions between lanthanide ions featuring strong spin–orbit coupling are rather complicated.[7] This limits the applicability of computational modelling at the same extent and reliability as it is used now for prediction

[a]*Leibniz Institute for Solid State and Materials Research, Helmholtzstraße 20, 01069 Dresden, Germany. E-mail: a.popov@ifw-dresden.de*
[b]*Center for Quantum Nanoscience, Institute for Basic Science (IBS), Seoul, Republic of Korea*
[c]*Department of Medicinal and Applied Chemistry, Kaohsiung Medical University, Kaohsiung 807, Taiwan*
[d]*Physik-Institut der Universität Zürich, Winterthurerstr. 190, CH-8057 Zürich, Switzerland*

†Electronic supplementary information (ESI) available. See DOI: 10.1039/d0qi00771d

of single-ion magnetic anisotropy in lanthanide molecular magnets.

Endohedral metallofullerenes (EMFs) encaging di-lanthanide clusters bridged *via* non-metal ions X^{q-}, such as N^{3-}, S^{2-}, C_2^{2-}, or O^{2-}, known as clusterfullerenes,[8] offer simple models for the studies of Ln···Ln interactions. Short Ln–X bonds lead to the strong magnetic anisotropy of Ln ions and the robust SMM behaviour in many Dy-clusterfullerenes.[2k,4d,9] The ligand-field (LF) splitting is usually so large that there is no mixing of LF and exchange states, thus simplifying the analysis and allowing to focus only on the exchange excitation in the ground state LF manifold. Note that quite a different situation is found in dimetallofullerenes featuring single-electron lanthanide–lanthanide bonds and hence giant exchange interactions,[5c,10] as well as in SMMs with radical bridges,[5a,b] but we will not consider such molecules in this work.

The first dinuclear EMF-SMM $Dy_2ScN@C_{80}$-I_h revealed the strong influence of Dy···Dy interactions on the magnetic hysteresis shape in comparison with mononuclear $DySc_2N@C_{80}$, and indicated a considerable ΔE_{AFM-FM} energy of *ca.* 6 cm^{-1}.[4d] Since then, we studied a number of di-nuclear EMFs and found a strong variation of the strength of Dy···Dy interactions in them. ΔE_{AFM-FM} in some of those studies was determined by fitting magnetization data.[4d,9h,k] In many cases it was also established that the relaxation of magnetization occurred *via* the exchange-excited state, showing Arrhenius behaviour with the barrier equal to ΔE_{AFM-FM}.[2k,4d,9b,c,h,i] Both approaches have certain limitations. The shape of magnetic susceptibility and isothermal magnetization curves is very sensitive to Ln···Ln interactions at low temperatures, but below the blocking temperature of magnetization, SMMs do not exhibit magnetic field and temperature dependence expected in the thermodynamic regime and thus cannot be used for a fitting, whereas higher-temperature curves are less sensitive to the Ln···Ln interaction parameters. Arrhenius barriers may be affected by the presence of concurrent relaxation mechanisms and also depend on the accuracy of the measured relaxation times. Note that determination of magnetization relaxation time τ_M is not straightforward when τ_M is longer than 10^4 s or falls into the gap between 0.1–1 s (the upper limit for AC magnetometry) and ~50 s (the lower accuracy limit for DC magnetometry).

Sub-Kelvin magnetization studies can be very useful for the determination of Ln···Ln interaction strength even when hysteresis sets in. Freezing thermal relaxation processes leaves QTM as the main relaxation mechanism. QTM takes places only at the level crossing and thus can give direct information on the interactions and avoids the need for fitting procedures. Such measurements were performed usually with ordered single crystals,[4a,11] but their utility for powder samples is not obvious since the distribution of orientations also leads to a distribution of level crossing positions. However, the recent sub-Kelvin magnetometry study of $Tb_2ScN@C_{80}$ (ref. 12) showed that the QTM-related features in magnetic hysteresis of a powder sample can be fairly sharp and may help in the careful description of the low-energy magnetic states in such dinuclear SMMs. Besides, such studies give access to magnetization relaxation dynamics, which would not be accessible otherwise. As mentioned, dinuclear EMF-SMMs often have thermally activated relaxation *via* the exchange-excited state down to 2 K. But how will the system behave if the temperature is low enough to freeze this process out? What is the time scale of the QTM process in which the coupled moment of two lanthanide ions flips as a single entity? In this work we apply sub-Kelvin magnetometry measurements to two isomers of sulfide clusterfullerene $Dy_2S@C_{82}$ to get a deeper insight into Dy···Dy interactions and its influence on the magnetic hysteresis and the relaxation of magnetization in these prototype dinuclear SMMs.

Results and discussion

Molecular structure and alignment of magnetic moments

Synthesis and structural characterization of two $Dy_2S@C_{82}$ isomers by single-crystal X-ray diffraction were described previously.[9c] Crystallographic studies revealed $C_s(6)$ and $C_{3v}(8)$ isomeric structures of the fullerene cage in two EMFs. These isomers share similar cage topology and are different only in the orientation of two pyracelene units highlighted in Fig. 1a. Pseudo-rotation of one CC bond in each pyracelene unit by 90° (known as Stone–Wales transformation) interconverts the fullerene cages.

Crystallographic studies gave the Dy–S bond lengths and Dy–S–Dy angles of 2.465(5), 2.518(5) Å and 98.3(2)° in the C_s isomer and 2.437(11), 2.511(9) Å and 94.4(2)° in the C_{3v} isomer. But significant disorder of the metal positions may affect these values. In the molecular structures optimized at the PBE-D level with PAW 4f-in-core potentials (VASP 5.0 code[13]) the Dy–S bond lengths and Dy–S–Dy angles are 2.484, 2.509 Å and 99.1° in the C_s isomer and 2.489, 2.506 Å and 97.4° in the C_{3v} isomer.

Strong uniaxial ligand field imposed by sulfide ion S^{2-} leads to the orientation of Dy magnetic moments along Dy–S bonds. Different mutual orientations of Dy moments in the dinuclear cluster Dy_2S give four states grouped into two quasi-doublets with a perpendicular orientation of the magnetic moment (Fig. 1b). The total magnetic moment of the molecule in each quasi-doublet depends on the Dy–S–Dy angle: $\mu_{FM} = 2\ \mu_{Dy}\cos(\alpha/2)$, $\mu_{AFM} = 2\ \mu_{Dy}\cdot\sin(\alpha/2)$, where μ_{Dy} is the magnetic moment of Dy^{3+} in the ground state, equal to $10\mu_B$, and α is the angle between quantization axes of Dy ions and is approximately equal to $\alpha \approx 180° - \angle$(Dy–S–Dy). The equality is not rigorous here because quantization axes of Dy ions may deviate slightly from the Dy–S bond directions. Thus, for the Dy–S–Dy angle of 105°, the μ_{FM} and μ_{AFM} moments are 12.2 and 15.9μ_B, respectively. In the following, the states with smaller and larger magnetic moments will be defined as antiferromagnetically (AFM) and ferromagnetically (FM) coupled. Note that this notation is rather arbitrary and for a Dy–S–Dy angle of 90° both moments would be equal. The preliminary study showed that the FM state in $Dy_2S@C_{82}$ is lower in energy than AFM.[9c]

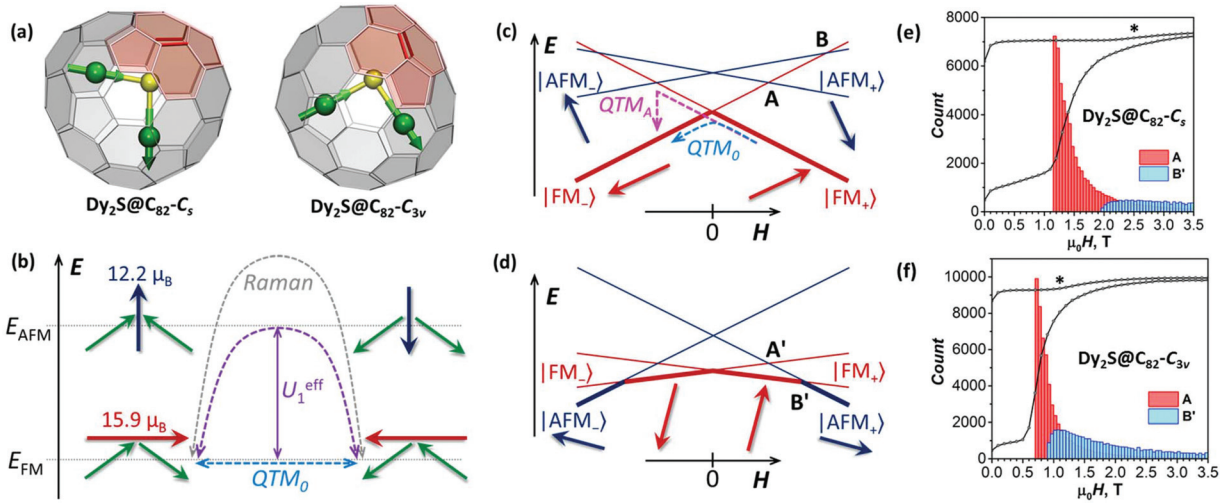

Fig. 1 (a) Molecular structures of $Dy_2S@C_{82}$-C_s and $Dy_2S@C_{82}$-C_{3v} (Dy is green, S is yellow, the carbon cage is transparent gray, and green arrows show one of the possible orientations of magnetic moments of Dy ions in the ground state doublet); two fullerene isomers have different orientation of pyracelene units highlighted in light red; C–C bonds which undergo 90° rotation in Stone–Wales transformation connecting these two isomers are shown in red. (b) Schematic description of two quasi-doublets defined as ferromagnetically (FM) and antiferromagnetically (AFM) coupled, green arrows denote magnetic moments of individual Dy ions, whereas red and dark blue arrows are total moment of the $Dy_2S@C_{82}$ molecule, the values are computed for the Dy–S–Dy angle of 105°; dashed arrows show the main low-temperature mechanisms of the relaxation of magnetization, including quantum tunneling of magnetization (QTM), Orbach mechanism *via* AFM-coupled state with effective barrier U_1^{eff}, and Raman mechanism *via* virtual state of higher energy. (c) and (d) show Zeeman diagrams for $Dy_2S@C_{82}$ for two arbitrary orientations of the molecule *versus* the magnetic field, in (c) the total magnetic moment of the FM state is close to the parallel orientation, whereas in (d) orientation is close to perpendicular; red and blue arrows show orientations of the magnetic moments for FM and AFM states, thick lines highlight the ground state in a given field range, and letters A, B, A′, and B′ mark different kinds of level crossing discussed in the text (each of these crossings is actually an avoided crossing with a certain tunneling gap, but showing this would overwhelm the figures with details). (e and f) Histograms (binning 0.05 T) of the crossing events of types A and B′ in C_s and C_{3v} isomers of $Dy_2S@C_{82}$ computed for an ensemble of 10^5 randomly oriented molecules overlaid with experimental hysteresis curves recorded at 0.41 K.

Magnetic hysteresis of $Dy_2S@C_{82}$ isomers. Magnetic hysteresis curves of $Dy_2S@C_{82}$-C_s and $Dy_2S@C_{82}$-C_{3v} are shown in Fig. 2.‡ The curves recorded at 0.41 K exhibit broad hysteresis with distinct features near zero field as well as at ±1.1 T (C_s isomer) and ±0.5 T (C_{3v} isomer). Measurements at 2 K give much narrower hysteresis, whereas the sharp features cannot be distinguished any more. For the C_s isomer, the hysteresis is closed completely between 2 and 3 K, while for the C_{3v} isomer a narrow opening is seen up to 4 K and disappears at 5 K.

The sharp features in low-T hysteresis curves can be associated with quantum tunnelling of magnetization (QTM). At low T, thermally activated relaxation processes become very slow, which makes relaxation of magnetization *via* QTM much more pronounced. As the QTM occurs at the avoided level crossing, it is necessary to understand the structure of the Zeeman diagram and possible types of level crossing events. Furthermore, the angular dependence of the Zeeman diagram needs to be understood because experimental studies are performed for powder samples with random orientation of molecules *versus* the external magnetic field. But first, it is necessary to determine the energy difference between the FM and AFM states.

‡The magnetization was measured in a Quantum Design MPMS3 vibrating sample magnetometer (VSM) with a ^{3}He cryostat.

Dy···Dy interactions in $Dy_2S@C_{82}$. To determine parameters of Dy···Dy coupling, magnetization curves of $Dy_2S@C_{82}$ isomers were fitted with the effective spin Hamiltonian in eqn (1):

$$\hat{H}_{\text{spin}} = \hat{H}_{\text{LF}_1} + \hat{H}_{\text{LF}_2} - 2j_{12}\hat{J}_1 \cdot \hat{J}_2 + \hat{H}_{\text{ZEE}} \quad (1)$$

where $\hat{H}_{\text{LF}_i}$ are single-ion ligand-field Hamiltonians of Dy^{3+} with *ab initio* computed parameters, j_{12} is the isotropic coupling constant between dysprosium moments, and $\hat{H}_{\text{ZEE}}$ is the Zeeman term. Dy^{3+} moments $\hat{J}_i$ are treated in the $|J,m_J\rangle$ basis sets of the $^6H_{15/2}$ multiplet. CASSCF(9,7)/SO-RASSI calculations reported earlier[9c] showed that the single-ion ground states of Dy^{3+} ions in both $Dy_2S@C_{82}$ isomers are almost pure states with m_J = ±15/2. The second Kramers doublet (KD) states are calculated to be 220–290 cm^{-1} higher in energy than the ground state. Thus, the low-temperature magnetization behaviour of $Dy_2S@C_{82}$ molecules is predominantly determined by the single J_z state of Dy^{3+} ions and their coupling giving a manifold of four states described in Fig. 1b, for which Hamiltonian in eqn (1) gives a reasonable description. The energy difference between FM and AFM-coupled states following from eqn (1) is $\Delta E_{\text{AFM–FM}} = 225j_{12}\cos(\alpha)$, where α is the angle between quantization axes of two Dy^{3+} ions as introduced above.

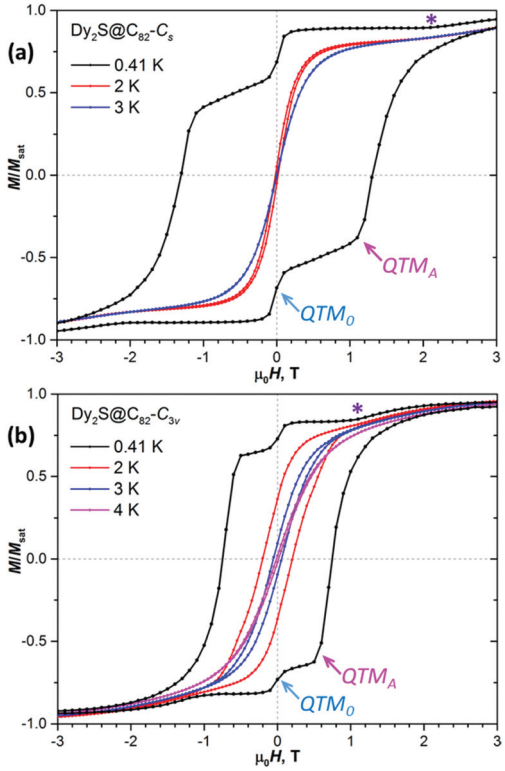

Fig. 2 Magnetic hysteresis of (a) $Dy_2S@C_{82}$-C_s and (b) $Dy_2S@C_{82}$-C_{3v} measured at T = 0.41 K and compared to some higher-temperature curves recorded until the hysteresis is closed. Sweep rates 2.9 mT s^{-1} for T = 2 K and above, and 3.3 mT s^{-1} for T = 0.41 K. QTM_0, QTM_A, and asterisk denote the features appearing because of the level crossing in Zeeman diagrams and are explained in the text.

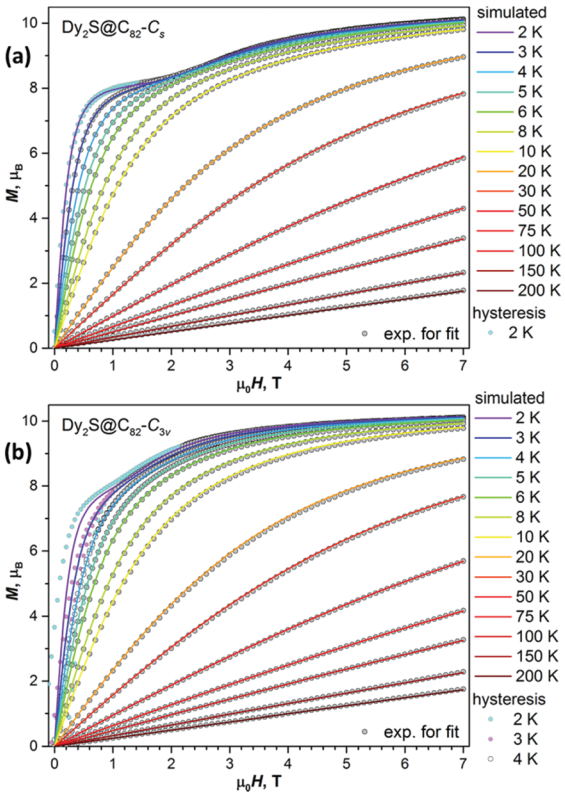

Fig. 3 Equilibrium magnetization curves of (a) $Dy_2S@C_{82}$-C_s and (b) $Dy_2S@C_{82}$-C_{3v} measured at temperatures between 2 K and 200 K. Grey dots are experimental values used in the fitting procedure; coloured lines are simulated for powder samples using fitted j_{12} and α parameters (j_{12} = 0.16 cm^{-1} and α = 72.3° for $Dy_2S@C_{82}$-C_s; j_{12} = 0.12 cm^{-1}, α = 75.7° for $Dy_2S@C_{82}$-C_{3v}). Coloured dots are the fragments of experimental magnetization curves with open hysteresis; these points were not used in the fitting procedure and are shown here to guide the eye. Note that the absolute experimental values of magnetization are not known because of the small sample mass, and the fitting is done for the normalized magnetization curves.

The coupling constant j_{12} and angle α are determined by fitting the experimental magnetization curves to eqn (1) taking powder-averaging into account using the PHI code[14] (Fig. 3). In both molecules, the FM coupling is found in the ground state. For $Dy_2S@C_{82}$-C_s, the best fit is obtained for j_{12} = 0.160 ± 0.001 cm^{-1} and α = 72.3 ± 0.1°, which gives ΔE_{AFM-FM} = 11.0 cm^{-1}. For $Dy_2S@C_{82}$-C_{3v}, the optimal j_{12} is 0.117 ± 0.002 cm^{-1} and α = 75.7 ± 0.3°, amounting to ΔE_{AFM-FM} = 6.4 cm^{-1}. Assuming that Dy^{3+} moments are aligned exactly along the Dy–S bonds, these fits give ∠(Dy–S–Dy) angles of 107.7° in C_s and 104.3° in C_{3v} isomers, which is somewhat higher than single-crystal values and DFT predictions for the lowest energy cluster positions. However, in real structures with disordered positions of Dy_2S clusters inside fullerenes, the ∠(Dy–S–Dy) angles are not single-valued, and the fits give only an average.

Level crossing, QTM, and shape of magnetic hysteresis in $Dy_2S@C_{82}$. With determined ΔE_{AFM-FM} values and angles between quantization axes of Dy^{3+} ions, Zeeman diagrams can be modelled at different angles between the external field and $Dy_2S@C_{82}$ molecules to better understand the features observed in hysteresis curves. The analysis below follows the approach applied recently in the study of the low-temperature hysteresis in $Tb_2ScN@C_{80}$.[12]

If magnetic field is aligned parallel to the magnetic moment of the FM (or AFM) state, only this state is split by the field, whereas the AFM (or FM) is not affected. The situation for an arbitrary orientation of the field is shown in Fig. 1c and d. In Fig. 1c, orientation of the total magnetic moment of the FM state is close to but not exactly parallel to the field direction. One of the FM doublet components is the ground state of the molecule in the whole field range ($|FM_+\rangle$ for $H > 0$ and $|FM_-\rangle$ for $H < 0$). The crossing at zero field causes the QTM within the FM doublet, $|FM_+\rangle \leftrightarrow |FM_-\rangle$ (denoted as QTM_0 in Fig. 1b, c and 2). In this process, magnetic moments of both Dy ions flip at once. This is a low-probability process and can be observed only at very low temperature, when faster thermal processes are frozen out. Indeed, a sharp but not strong drop of magnetization can be seen upon zero field crossing in 0.41 K hysteresis curves of both $Dy_2S@C_{82}$ isomers, but this feature is not seen at 2 K and above (Fig. 2).

Another level crossing event of high importance for the understanding of the hysteresis shape is denoted as type A in

Fig. 1c. It corresponds to the crossing of the higher-energy FM state with a lower-energy AFM state (*e.g.*, the crossing of $|FM_+\rangle$ with $|AFM_-\rangle$ in the negative field, or $|FM_-\rangle$ with $|AFM_+\rangle$ in the positive field). Consider evolution of the system in Fig. 1c when the magnetic field is swept from large positive to large negative values. At $H > 0$, $|FM_+\rangle$ is the ground state and magnetization is slowly decreasing because of the partial population of other states. At low temperatures, when the thermal relaxation is very slow, magnetization remains almost constant until zero field. During zero-field crossing, the $|FM_+\rangle$ state can relax to the $|FM_-\rangle$ state by the QTM_0 mechanism. Fig. 2 shows that only ~15–20% of $Dy_2S@C_{82}$ molecules undergoes the QTM_0 and adopts the $|FM_-\rangle$ state after crossing zero field, whereas the large part remains in the $|FM_+\rangle$ state, resulting in the positive magnetization in the negative field. For this large part of $Dy_2S@C_{82}$ molecules, the fast relaxation of magnetization is triggered at the next level crossing of type A between $|FM_+\rangle$ and $|AFM_-\rangle$ states (also denoted as QTM_A in Fig. 1c and 2). The $|FM_+\rangle \rightarrow |AFM_-\rangle$ transition appears to be much more efficient than $|FM_+\rangle \rightarrow |FM_-\rangle$ as evidenced by the abrupt drop of magnetization to negative values beyond the level crossing. It is not clear yet if the QTM_A event results in a concerted relaxation to the $|FM_-\rangle$ state,[4b,12] or that the $|AFM_-\rangle$ state is accessed first and then gradually relaxes to the $|FM_-\rangle$ state. But the second option would require a thermally activated mechanism, and hence the concerted mechanism is more probable. If after crossing of type A, a part of the molecules still stays in the $|FM_+\rangle$ state, the next crossing would be of type B with the $|AFM_+\rangle$ state. It may also trigger the change of the magnetization *via* $|FM_+\rangle \rightarrow |AFM_+\rangle$ transition, but we do not see corresponding features in hysteresis curves (Fig. 2). Presumably, relaxation of magnetization at the level crossing of type A is very efficient, and the fraction of $Dy_2S@C_{82}$ molecules surviving in the $|FM_+\rangle$ state beyond this level crossing is very small.

Another possibility not considered yet in our analysis is that the magnetic field is oriented nearly perpendicular to the magnetic moment of the FM state. In this case, $|AFM_+\rangle$ and $|AFM_-\rangle$ may become ground states at some large positive and negative fields, respectively (Fig. 1d). Upon reducing the field, $|FM_{+,-}\rangle$ states become lower in energy than $|AFM_{+,-}\rangle$ giving the level crossing of type B′ (Fig. 1d). Again, a stepwise drop of magnetization is possible at this crossing following the $|AFM_+\rangle \leftrightarrow |FM_+\rangle$ and $|FM_-\rangle \leftrightarrow |AFM_-\rangle$ transitions, but it cannot be as pronounced as for type A because the fraction of molecules undergoing this type of crossing in the available field range of $[-7, 7]$ T is relatively small as discussed below. The change of magnetization at the level crossing of type B′ should also occur in the thermodynamic regime, when the relaxation of magnetization is fast. Corresponding features can be identified in magnetization curves recorded below 3–4 K (Fig. 3).

Powder samples such as studied in this work have molecules in different orientations. Therefore, the level crossing event of each type will not occur in one particular field but will be distributed over a certain field range. Depending on the shape of this distribution, QTM features in hysteresis curves may appear as sharp or smeared. To analyse the distributions, we used j_{12} and α parameters determined from the fits to experimental magnetization curves and calculated level crossing positions for $Dy_2S@C_{82}$ molecules with 10^5 different orientations of the magnetic field vector around them uniformly distributed on the Fibonacci sphere.§ Fig. 1e and f show histograms of level crossing events of types A and B′ for C_s and C_{3v} isomers of $Dy_2S@C_{82}$ in the field range of 0–3.5 T.

For $Dy_2S@C_{82}$-C_s, 58.3% molecules have the crossing of type A between 0 and 7 T, and 42% of these crossings happen between 1.16 and 1.36 T. Likewise, 57.5% of $Dy_2S@C_{82}$-C_{3v} molecules undergo this type of crossing between 0 and 7 T, and 54% of those events fall into the narrow field range between 0.72 and 0.92 T. Thus, crossing events of type A have a very sharp distribution with the asymmetric peak near the smallest field, at which this event can take place. This threshold field (H_A) is simply proportional to the energy difference between AFM and FM states:

$$\mu_0 H_A[T] = \frac{\Delta E_{AFM-FM}}{2\mu_{Dy}} = 1.07\frac{\Delta E_{AFM-FM}[cm^{-1}]}{\mu_{Dy}[\mu_B]}, \qquad (2)$$

where $\mu_0 H_A$ is in Tesla, ΔE_{AFM-FM} in cm^{-1}, and $\mu_{Dy} = 10\mu_B$ is magnetic moment of a Dy^{3+} ion in $Dy_2S@C_{82}$, and the numerical coefficient appears because of the unit conversion. The very high density of crossing events near this threshold field translates into sharp QTM_A features in the magnetic hysteresis curves (Fig. 1 and 2), which allows accurate estimation of ΔE_{AFM-FM}. Importantly, the determination of ΔE_{AFM-FM} from the QTM_A field for powder samples does not involve the angle between magnetic moments of Dy^{3+} ions α and is not affected by the powder averaging. Note that unlike the crossing of type B′ discussed below, the crossing of type A is an intrinsic SMM feature and can be observed in magnetization curves only when relaxation of magnetization near zero field is slow enough to enable a significant non-equilibrium fraction of molecules in the state $|FM_+\rangle$ in the negative field or in the state $|FM_-\rangle$ in the positive field.

The crossing of type B′, on the other hand, has a less distinct position (Fig. 1e and f). For $Dy_2S@C_{82}$-C_s, 25% of all molecules have this kind of crossing in the field range below 7 T. The smallest field, in which the crossing can take place, is 1.95 T, and the next 0.5 T (1 T) range includes only 16% (33%) of events among the molecules with the B′ point below 7 T. For $Dy_2S@C_{82}$-C_{3v}, the distribution is slightly denser. The fraction of all molecules with B′ crossing below 7 T is 32%, of that 22% (43%) have this crossing in the range of 0.5 T (1 T) above the threshold field of 1.14 T. Thus, in contrast to type A, the crossing of type B′ occurs with a smaller fraction of molecules (hence smaller change of magnetization), and the distribution

§ The ensemble of Zeeman diagrams was computed for 10^5 different orientations of the magnetic field vectors evenly spaced along with the Fibonacci sphere grid points, assuming Hamiltonian eqn (1). The massive data were generated and analyzed using in-house Python scripts while the Hamiltonian eigenproblems were solved using the PHI code.[14]

of the events in the field scale is much broader. Although the corresponding deflection can be seen in the experimental curves (marked with an asterisk in Fig. 1e, f and 2), we cannot determine if this feature occurs because of the QTM-induced relaxation at the level crossing, or because the system simply follows a thermodynamic regime. The lowest field, at which B′ crossing can take place, is defined in eqn (3):

$$\mu_0 H_{B'}\,[T] = \frac{\Delta E_{AFM-FM}}{2\mu_{Dy}\sin(\alpha/2)} = 1.07\frac{\Delta E_{AFM-FM}[cm^{-1}]}{\mu_{Dy}[\mu_B]\sin(\alpha/2)} = \frac{\mu_0 H_A}{\sin(\alpha/2)}, \quad (3)$$

Eqn (3) also allows determination of ΔE_{AFM-FM} if α is known or can be estimated from the known ∠(Dy–S–Dy) angle. But because of the broad distribution of crossing events in powder samples, and because the maximum in the distribution is shifted from the threshold field $H_{B'}$ (Fig. 1e and f), the corresponding features in magnetization curves are very smeared, and precision of the ΔE_{AFM-FM} value estimated this way for powder samples would be not very high. Anyway, analogs of formulae (3) were used earlier for estimation of exchange interaction in powder samples, mainly for dinuclear complexes with the AFM ground state.[4e,15] For oriented single crystals though, the value can be quite accurate.[4a,11]

Magnetization relaxation times. Low-temperature magnetic studies allowed the determination of magnetization relaxation times and a more complete description of magnetization dynamics in $Dy_2S@C_{82}$ isomers. Fig. 4 shows the temperature dependence of zero-field relaxation times (τ_M) in the whole available temperature range, including the data determined by recording decay curves with DC magnetometry in this work and relaxation times determined by AC magnetometry earlier in ref. 9*c*. Both isomers exhibit several distinct relaxation regimes, which are described by a combined equation:

$$\tau_M^{-1}(T) = \tau_{QTM}^{-1} + CT^n + \sum_i \tau_{0i}^{-1}\exp(-U_i^{eff}/T), \quad (4)$$

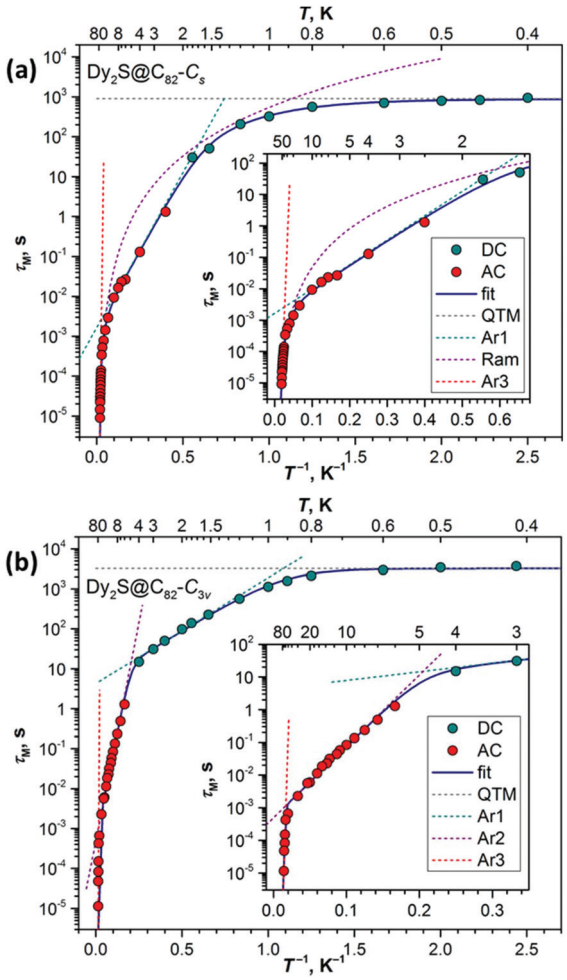

Fig. 4 Magnetization relaxation times of (a) $Dy_2S@C_{82}$-C_s and (b) $Dy_2S@C_{82}$-C_{3v}. Dark cyan and red dots are DC and AC measurements, solid lines are fits by a combined equation eqn (1), and dashed lines are contributions of QTM, Raman, and Arrhenius processes. The insets show magnification of higher-temperature parts.

where τ_{QTM} is the QTM relaxation time, the second term describes the relaxation of magnetization *via* the Raman mechanism, and the third term describes one or more Arrhenius regimes. Using the DC measurements from this work and earlier AC data, we refitted the τ_M-T^{-1} dependencies.

At the lowest temperatures, relaxation time tends to level off, which indicates a transition to the QTM relaxation regime. Characteristic QTM times obtained from the fits are 906 ± 80 s for the C_s isomer and 3224 ± 418 s for the C_{3v} isomer. These rather long times explain why the QTM_0 regime can be observed in hysteresis curves only at sub-Kelvin temperature. Consider the FM ground-state of a dinuclear Dy system such as shown in Fig. 1b. If a magnetic moment of one of the metal ions is flipped, the system arrives at the AFM state, which has higher energy. Thus, the ΔE_{AFM-FM} difference prevents zero-field QTM with the flipping of one Dy^{3+} moment. At the same time, it allows the thermally activated relaxation process with the barrier U_1^{eff} equal to ΔE_{AFM-FM} (Fig. 1b). We observed this kind of mechanism in many di-nuclear EMFs studied before,[2k,4d,9b,c,h,i,k,12] and it can be also recognized in $Dy_2S@C_{82}$. For the C_s isomer, this mechanism dominates between 2 and 10 K, the U_1^{eff} barrier is 17.9 ± 0.5 K, whereas attempt time τ_{01} is 1.6 ± 0.2 ms. In the C_{3v} isomer, the barrier is lower, U_1^{eff} = 6.1 ± 0.4 K, but attempt time is much longer, τ_{01} = 4 ± 1 s, and the mechanism is operative between 1 and 4 K. Thus, only the use of sub-K temperatures in this work allowed freezing out the Orbach relaxation *via* the AFM state and we observed the $|FM_+\rangle \leftrightarrow |FM_-\rangle$ QTM regime, in which the whole magnetic moment of the $Dy_2S@C_{82}$ molecule flips at once (Fig. 1b).

At higher temperature, the mechanism of relaxation changes to Raman in the C_s isomer with C = (1.8 ± 3) 10^{-3} s^{-1} K^{-n}, n = 4.0 ± 0.1. For C_{3v} we observe instead another Arrhenius process, with U_2^{eff} of 50 ± 2 K and τ_{02} of (4.9 ± 0.7) 10^{-4} s. The Raman mechanism with a strong coupling to certain low frequency vibration modes, such as endohedral

cluster vibrations, is likely to be the reason for this linear regime.[16] These Raman mechanisms govern relaxation of magnetization of $Dy_2S@C_{82}$ up to 40–50 K. Above this temperature, another change of the relaxation mechanism takes place for the C_{3v} isomer. This time the Orbach mechanism with the relaxation *via* ligand-field excited states of Dy^{3+} ions is likely to play the main role, and we obtain the barrier as high as 1569 ± 180 K. For the C_s isomer the fitting at high temperature is more ambiguous (see Fig. S6†). Similar to the C_{3v} isomer, we can also invoke one more Arrhenius process, which would have a barrier of 683 ± 83 K. At the same time, the Raman process alone also gives a reasonable description of the data. But since the χ'' signal by these temperatures dropped dramatically and the values were obtained at the limit of the magnetometer sensitivity, the reliability of the determined relaxation times is unfortunately low, which also affects stability and reliability of the fit. We thus prefer to restrain from the further discussion of these barriers.

Dy···Dy interactions in $Dy_2S@C_{82}$ and comparison to other dinuclear Dy molecular magnets. In this work we could make estimations of ΔE_{AFM-FM} in $Dy_2S@C_{82}$ by three independent methods: from the QTM_A features in sub-Kelvin magnetic hysteresis curves (Fig. 2), from the fit of magnetization curves (Fig. 3), and as the barrier U_1^{eff} in the low-temperature Arrhenius regime (Fig. 4). The values for the two isomers are compared in Table 1. For the C_s isomer, we observe a good agreement of all three methods, giving the numbers in the range of 10.7–12.4 cm^{-1}. For the C_{3v} isomer, the absolute value is smaller and hence the difference between estimations of 4.2 cm^{-1} from U_1^{eff} to 6.4 cm^{-1} from the fit of magnetization curves is comparably large. The latter seems to be an overestimation since the distribution of crossing events computed with the ΔE_{AFM-FM} value from the fit of *M–H* curves has the maximum at a somewhat higher field than the QTM_A feature in the hysteresis curve (Fig. 1f). Overall, estimation of the ΔE_{AFM-FM} value from the QTM_A features in sub-Kelvin hysteresis appears to be the most straightforward and reliable. A possible contribution of other relaxation mechanisms or errors in the determined relaxation times can affect the U_1^{eff} value, whereas the fit of magnetization curves in the case of open magnetic hysteresis has to rely on higher-temperature data, which are less sensitive to the value of ΔE_{AFM-FM}.

The Dy···Dy coupling energy can be further divided into exchange and dipolar contributions, ΔE_{AFM-FM}^{exch} and ΔE_{AFM-FM}^{dip}. The dipolar term can be computed exactly when the Dy···Dy distance and orientation of magnetic moments are known. Using the angle from the fit of magnetization curves and Dy–S bond lengths from DFT calculations, ΔE_{AFM-FM}^{dip} values are estimated as 2.2 cm^{-1} in C_s and 2.3 cm^{-1} in C_{3v} isomers. ΔE_{AFM-FM}^{exch}, calculated as the difference between total and dipolar interaction energies, therefore is 8.5 cm^{-1} in C_s and 2.8 cm^{-1} in C_{3v} isomers (the total energy estimated from hysteresis is used hereafter).

Table 2 compares the values of ΔE_{AFM-FM}, ΔE_{AFM-FM}^{dip}, and ΔE_{AFM-FM}^{exch} from this work to those of other dinuclear Dy metallofullerenes studied earlier,[9c,h,i,k] including Dy_2O, Dy_2C_2 and Dy_2MN (M = Sc, Lu) clusterfullerenes with bridging O^{2-}, C_2^{2-}, and N^{3-} units. Nitride and carbide clusterfullerenes also exhibited FM interactions between Dy ions, $Dy_2C_2@C_{82}$ showing the largest ΔE_{AFM-FM} value of 12.1 cm^{-1} (determined from U_1^{eff} in ref. 9*c*). The ΔE_{AFM-FM} energy in $Dy_2S@C_{82}$-C_s is comparable to this value. Oxide clusterfullerenes with Dy_2O clusters tend to show AFM or weak to negligible FM interactions, $Dy_2O@C_{82}$-C_{2v} featuring the largest ΔE_{AFM-FM} gap of −12.9 cm^{-1}. Importantly, all EMF-SMMs have very similar ΔE_{AFM-FM}^{dip} energies, and large variations in total Dy···Dy interaction energies across different EMF types are caused by the strong variation of the exchange term.

Table 1 Parameters of Dy···Dy interactions in $Dy_2S@C_{82}$ isomers determined by different methods[a]

EMF	ΔE_{hyst}	U_1^{eff}	ΔE_{fit}	α_{fit}
$Dy_2S@C_{82}$-C_s	10.7 ± 0.5	12.4 ± 0.4	11.0	72.3 ± 0.1
$Dy_2S@C_{82}$-C_{3v}	5.1 ± 0.5	4.2 ± 0.3	6.4	75.7 ± 0.3

[a] ΔE_{hyst}, U_1^{eff}, and ΔE_{fit} are estimations of ΔE_{AFM-FM} (in cm^{-1}), respectively, from the QTM_A feature in sub-Kelvin hysteresis (Fig. 2), from the Arrhenius regime in relaxation times (Fig. 4), and from the fit of magnetization curves (Fig. 3). The latter also gives α_{fit} as the angle between magnetic moments of Dy^{3+} ions

Table 2 Energies and pseudospin coupling constants of Dy···Dy interactions in $Dy_2S@C_{82}$ isomers compared to those in some other dinuclear EMF-SMMs and $\{Dy_2\}$ compounds[a]

EMF[b]	ΔE^{tot}	ΔE^{dip}	ΔE^{exch}	J_{tot}	J_{dip}	J_{exch}
$Dy_2S@C_{82}$-C_s	10.7	2.2	8.5	70.4	14.4	56.0
$Dy_2S@C_{82}$-C_{3v}	5.1	2.3	2.8	41.3	18.5	22.8
$Dy_2O@C_{72}$-C_s	1.5	3.0	−1.5	4.0	8.0	−4.0
$Dy_2O@C_{74}$-C_2	~0.1	2.6	−2.5	0.2	5.1	−4.9
$Dy_2O@C_{82}$-C_s	−7.5	3.0	−10.5	−23.3	9.3	−32.6
$Dy_2O@C_{82}$-C_{3v}	−5.4	2.5	−7.8	−21.6	10.2	−31.8
$Dy_2O@C_{82}$-C_{2v}	−12.9	2.6	−15.6	−41.9	8.6	−50.5
$Dy_2C_2@C_{82}$-C_s	12.1	2.6	9.5	64.4	13.6	50.8
$Dy_2ScN@C_{80}$-I_h	5.6	3.3	2.3	24.9	14.5	10.4
$Dy_2LuN@C_{80}$-I_h	3.0	3.3	−0.3	12.6	14.0	−1.4
$\{Cp'_2Dy(\mu\text{-}SR)\}_2$	−2.0			−4.4	−2.2	−2.2
$\{Dy_2O_2\}$-**A**	7.0			15.0	5.5	9.5
$\{Dy_2O_2\}$-**B**	6.0			11.4	4.6	6.8
$\{Dy_2O_2\}$-**C**	−5.3			−11.0	−2.7	−8.4

[a] ΔE^{tot} is ΔE_{AFM-FM} (in cm^{-1}), whereas ΔE^{dip} and ΔE^{exch} are dipolar and exchange contributions, respectively, and ΔE^{exch} is computed as $\Delta E^{tot} - \Delta E^{dip}$; J_{tot}, J_{dip} and J_{exch} are pseudospin coupling constants (in cm^{-1}) from eqn (5). [b] ΔE^{tot} for $Dy_2S@C_{82}$ is determined from hysteresis in this work, or as U_1^{eff} for $Dy_2O@C_{2n}$ (ref. 9*i* and *k*), $Dy_2C_2@C_{82}$ (ref. 9*c*), and $Dy_2MN@C_{80}$ (ref. 9*h*). In $\{Cp'_2Dy(\mu\text{-}SR)\}_2$ from ref. 17, R = $SiPh_3$; $\{Dy_2O_2\}$-**A** is $[Dy_2(dbm)_2(LH_2)_2]\cdot H_2O$ from ref. 18 (LH_3 = (1E,3E)-2-hydroxy-5-methylisophthalaldehyde dioxime, Hdbm = dibenzoylmethane); $\{Dy_2O_2\}$-**B** is $[Dy(L)Cl(CH_3OH)]_n$ from ref. 19 (H_2L = *N*′-(5-bromo-2-hydroxybenzylidene)pyrazine-*N*-oxide-carbohydrazide); $\{Dy_2O_2\}$-**C** is $[Dy_2(a'povh)_2(OAc)_2(DMF)_2]$ from ref. 20 ($H_2a'povh$ = *N*′-[amino (pyrimidin-2-yl)methylene]-*o*-vanilloyl hydrazine).

To put these values into a broader context of di-lanthanide molecular magnets, we took into account that the most frequently used approach to describe Dy···Dy interactions nowadays employs the pseudospin model popularized by Ungur and Chibotaru in their POLY_ANISO code.[21] The ground magnetic state of Dy^{3+} ions is described as a pseudospin $\tilde{s}$ = 1/2 with a highly anisotropic *g*-tensor (close to (0, 0, 20) for the Kramers doublet with dominant m_J = ±15/2 term), and the pseudospin exchange Hamiltonian within the Lines model[22] takes the form of eqn (3):

$$\hat{H}_{\text{exch}} = -J_{\text{tot}}\hat{\tilde{s}}_1 \cdot \hat{\tilde{s}}_2 = -(J_{\text{dip}} + J_{\text{exch}})\hat{\tilde{s}}_1 \cdot \hat{\tilde{s}}_2 \quad (5)$$

With this Hamiltonian, $\Delta E_{\text{AFM–FM}} = 0.5J_{\text{tot}}\cos(\alpha)$, and hence $J_{\text{tot}} = 450j_{12}$ (where j_{12} is the coupling constant from eqn (1)). The calculated J_{tot}, J_{dip}, and J_{exch} constants for dinuclear EMF-SMMs are listed in Table 2. The J_{tot} and J_{exch} values of $Dy_2S@C_{82}$-C_s, 70.4 and 56.0 cm^{-1}, are the largest among all EMF-SMMs.

We are aware of only two molecular magnets with sulfur-bridged Dy ions other than the $Dy_2S@C_{82}$: Dy_4 complex with thiolate ligand bridges,[23] and the dinuclear complex with $Dy(Cp')_2$ units bridged *via* two (μ-$SSiPh_3$) groups.[17] In both systems, Dy···Dy coupling is weakly AFM as can be assumed based on the shape of χT curves. The $\Delta E_{\text{AFM–FM}}$ and J_{tot} values in $\{Cp'_2Dy(\mu\text{-}SSiPh_3)\}_2$ are −2 and −4.4 cm^{-1}, respectively.

The μ_2-O bridges are much more common than μ_2-S in dinuclear Dy molecular magnets, especially in the form of $\{Dy_2O_2\}$ fragments. For those, we found only three compounds with $|J_{\text{tot}}|$ exceeding 10 cm^{-1} (Table 2; see ref. 9*i* for a recent survey of Dy···Dy interaction parameters in $\{Dy_2O_2\}$ compounds). Two of them have phenoxide bridges with FM coupling and J_{tot} values of 15.0 and 11.4 cm^{-1}.[18,19] In the complex with vanilloyl bridges, the coupling is AFM and J_{tot} is −11 cm^{-1}.[20] Table 2 shows that in EMF-SMMs the range of coupling constants can be several times larger. This large difference in J_{tot} constants may appear somewhat misleading because the $\Delta E_{\text{AFM–FM}}$ values also depend on the angle between Dy axes. In EMF-SMMs, magnetic moments of Dy ions are usually non-collinear, so the range of the energies is not as high as for the coupling constants. But still, $\Delta E_{\text{AFM–FM}}$ energies in EMF-SMMs can be considerably larger than those in other $\{Dy_2\}$ molecular magnets.

One reason for this lies in the comparably strong dipolar interactions between Dy moments in EMFs caused by the relatively short Dy···Dy distance and suitable Dy–X–Dy angles maximizing dipolar interactions. Yet in many $\{Dy_2O_2\}$ compounds, the distances are even shorter than those in EMFs. Thus, we conclude that the exchange interactions between Dy moments in EMFs are mainly responsible for these unprecedentedly strong Dy···Dy interactions in EMFs. The reasons for this strong exchange are not clear yet. Short Dy–X bonds leading to enhanced superexchange *via* the bridging atoms may be one of the reasons. But this factor cannot explain why variation of exchange coupling can be so strong in different cage isomers,

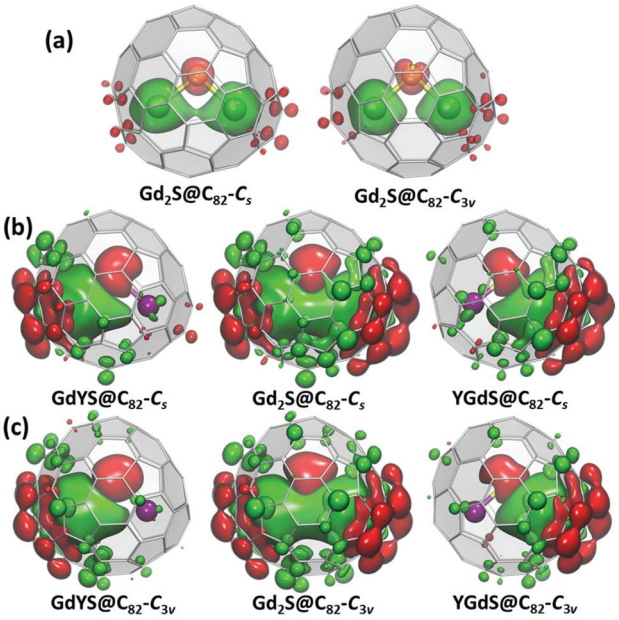

Fig. 5 DFT-computed spin-density distribution (green – "+", red – "–") in: (a) $Gd_2S@C_{82}$-C_s and $Gd_2S@C_{82}$-C_{3v} molecules shown with isovalues of ±0.0012 a. u. (b) $Gd_2S@C_{82}$-C_s and $GdYS@C_{82}$-C_s with an isovalue of ±0.00012 a. u. (c) $Gd_2S@C_{82}$-C_{3v} and $GdYS@C_{82}$-C_{3v} with an isovalue of ±0.00012 a. u. The isosurfaces in (a) are plotted semitransparent to show positions of metals and sulfur in the endohedral cluster. Computations performed at the PBE0/TZVP level with DKH scalar-relativistic correction and DKH-tailored full-electron basis sets.

such as that found in this work for C_s and C_{3v} isomers of $Dy_2S@C_{82}$ or observed earlier for isomers of $Dy_2O@C_{82}$.[9i]

Evidently, the fullerene cage in EMF-SMMs should not be considered as just a container for magnetic species. We suggest that the interaction between Dy ions is also affected through the spin polarization of the fullerene π-system in the spirit of the Ruderman–Kittel–Kasuya–Yosida (RKKY) mechanism of interaction between magnetic atoms *via* conduction electrons in metals.[24] For instance, the RKKY mechanism explains oscillatory distance dependence of interactions between magnetic adatoms in graphene, an infinite limit of the fullerene π-system.[25] Fig. 5 plots spin density distribution in $Gd_2S@C_{82}$ (S = 15) and $GdYS@C_{82}$ (S = 8) molecules computed at the PBE0 level with full-electron basis sets.¶ The use of Gd instead of Dy in these calculations allows the application of a single-determinant DFT approach and limits the focus to spin-only contribution to the Ln···Ln exchange interactions; spin–orbit coupling effects cannot be captured by this simple approach. Calculations for $Gd_2S@C_{82}$ also allow using broken-symmetry DFT to estimate the exchange coupling between Gd magnetic moments (see ref. 9*c* and ESI†), but such results cannot be directly transferred to Dy analogs.

¶DFT calculations for $Gd_2S@C_{82}$ and $GdYS@C_{82}$ molecules were performed with the Orca 4.2.1 suite[26] using the PBE0 functional, DKH scalar-relativistic correction, and SARC-TZVP basis sets.[27] Spin-densities are visualized with VMD.[28]

When the isovalues of ±0.0012 a. u. are used in plotting the spin density (ρ_{spin}) isosurfaces, the surface with positive ρ_{spin} (coloured green in Fig. 5a) encompasses two Gd atoms as can be expected for the state with spin multiplicity of $S = 15$. At the same time, a pronounced negative spin polarization of the bridging sulfur is also well seen. Obviously, superexchange *via* the μ_2-S atom should be considerable in these systems. Besides, the negative spin polarization of fullerene carbon atoms closest to Gd is also visible. The plots with lower spin density isovalues of ±0.00012 a. u. show that spin polarization of carbon atoms with alternating sign extends over the whole fullerene cage. The negative spin polarization of carbons near Gd is changed to the positive one for more distant carbons. Interestingly, although the cage spin polarization patterns calculated for GdYS@C_{82} molecules resemble closely halves of spin-density plots in Gd_2S@C_{82}, they are not completely identical (Fig. 5b and c). Besides, Gd-induced spin polarization of the cage carbons in GdYS@C_{82} extends to the half of the cage not coordinated to Gd. Thus, there should be non-negligible through-cage interaction between endohedral lanthanide ions. It is reasonable to suggest that through-cage spin–spin interaction pathways should depend on the topology of the fullerene π-systems, and thus be different from cage to cage even when structural parameters of the endohedral cluster are very similar. Further exploration of this effect is worth a detailed study but goes beyond the scope of this work.

Conclusions

In this work, we performed a study of Dy⋯Dy magnetic interactions and low-temperature relaxation dynamics in Dy_2S@C_{82} as a prototype dinuclear SMM with a ferromagnetically coupled ground state. Although the study is performed on powder samples, the broad sub-Kelvin magnetic hysteresis with clear QTM steps observed for both cage isomers of Dy_2S@C_{82} appeared instrumental for the determination of the energy difference between the FM and AFM states. Comparison with the values determined by other approaches, such as fitting of magnetization data or the energy barrier of the Arrhenius relaxation process, showed reasonable agreement. Comparison to other dinuclear SMMs revealed that the $C_s(6)$ isomer of Dy_2S@C_{82} features one of the highest Dy⋯Dy coupling strength values ever reported. Furthermore, the two-fold variation of the Dy⋯Dy coupling strength between two cage isomers is found. This variation cannot be explained by the difference in the structural parameters of the Dy_2S cluster in two structures and points to a possibility of the indirect exchange interactions between lanthanide ions *via* the fullerene π-system.

Measurements of the magnetization relaxation time at sub-Kelvin temperatures also allowed achieving a relaxation regime not observed in dinuclear EMF-SMMs before. Typically, the main low-temperature relaxation mechanism in these compounds is the Orbach process with the barrier corresponding to the energy difference between FM and AFM states. In Dy_2S@C_{82} this mechanism is observed down to 1–2 K. But below 1 K, this thermally activated process becomes inefficient, giving way to quantum tunnelling with the simultaneous flip of two Dy moments.

Conflicts of interest

There are no conflicts to declare.

Acknowledgements

The authors acknowledge funding from the European Union's Horizon 2020 research and innovation programme, European Research Council (grant agreement no. 648295 to A. A. P.), Marie Skłodowska-Curie action (grant agreement no. 748635 to S. M. A.), the Deutsche Forschungsgemeinschaft (grants PO 1602/4-1 and 1602/5-1 to A. A. P.) and the Swiss National Science Foundation (Projects No. 200021L_147201 and No. 206021_- 150784 to T. G.). We appreciate the help from Dr Anja U. B. Wolter and Sebastian Gaß in magnetic measurements and Ulrike Nitzsche for the help with computational resources in IFW Dresden.

Notes and references

1 (*a*) K. L. M. Harriman, D. Errulat and M. Murugesu, Magnetic Axiality: Design Principles from Molecules to Materials, *Trends Chem.*, 2019, **1**, 425; (*b*) A. K. Bar, P. Kalita, M. K. Singh, G. Rajaraman and V. Chandrasekhar, Low-coordinate mononuclear lanthanide complexes as molecular nanomagnets, *Coord. Chem. Rev.*, 2018, **367**, 163; (*c*) J.-L. Liu, Y.-C. Chen and M.-L. Tong, Symmetry strategies for high performance lanthanide-based single-molecule magnets, *Chem. Soc. Rev.*, 2018, **47**, 2431; (*d*) E. Bartolomé, A. Arauzo, J. Luzón, J. Bartolomé and F. Bartolomé, in *Handbook of Magnetic Materials*, ed. E. Brück, Elsevier, 2017, p. 1; (*e*) Z. Zhu, M. Guo, X.-L. Li and J. Tang, Molecular magnetism of lanthanide: Advances and perspectives, *Coord. Chem. Rev.*, 2019, **378**, 350; (*f*) S. T. Liddle and J. van Slageren, Improving f-element single molecule magnets, *Chem. Soc. Rev.*, 2015, **44**, 6655; (*g*) P. Zhang, L. Zhang and J. Tang, Lanthanide single molecule magnets: Progress and perspective, *Dalton Trans.*, 2015, **44**, 3923.

2 (*a*) L. Ungur and L. F. Chibotaru, Ab Initio Crystal Field for Lanthanides, *Chem. – Eur. J.*, 2017, **23**, 3708; (*b*) L. Ungur and L. F. Chibotaru, Strategies toward High-Temperature Lanthanide-Based Single-Molecule Magnets, *Inorg. Chem.*, 2016, **55**, 10043; (*c*) T. Pugh, N. F. Chilton and R. A. Layfield, A Low-Symmetry Dysprosium Metallocene Single-Molecule Magnet with a High Anisotropy Barrier, *Angew. Chem., Int. Ed.*, 2016, **55**, 11082; (*d*) Y.-S. Ding, N. F. Chilton, R. E. P. Winpenny and Y.-Z. Zheng, On

Approaching the Limit of Molecular Magnetic Anisotropy: A Near-Perfect Pentagonal Bipyramidal Dysprosium(III) Single-Molecule Magnet, *Angew. Chem., Int. Ed.*, 2016, **55**, 16071; (*e*) F.-S. Guo, B. M. Day, Y.-C. Chen, M.-L. Tong, A. Mansikkamäki and R. A. Layfield, Magnetic hysteresis up to 80 kelvin in a dysprosium metallocene single-molecule magnet, *Science*, 2018, **362**, 1400; (*f*) F.-S. Guo, B. M. Day, Y.-C. Chen, M.-L. Tong, A. Mansikkamäki and R. A. Layfield, A Dysprosium Metallocene Single-Molecule Magnet Functioning at the Axial Limit, *Angew. Chem., Int. Ed.*, 2017, **56**, 11445; (*g*) Y.-C. Chen, J.-L. Liu, L. Ungur, J. Liu, Q.-W. Li, L.-F. Wang, Z.-P. Ni, L. F. Chibotaru, X.-M. Chen and M.-L. Tong, Symmetry-Supported Magnetic Blocking at 20 K in Pentagonal Bipyramidal Dy(III) Single-Ion Magnets, *J. Am. Chem. Soc.*, 2016, **138**, 2829; (*h*) J. Liu, Y.-C. Chen, J.-L. Liu, V. Vieru, L. Ungur, J.-H. Jia, L. F. Chibotaru, Y. Lan, W. Wernsdorfer, S. Gao, X.-M. Chen and M.-L. Tong, A Stable Pentagonal Bipyramidal Dy(III) Single-Ion Magnet with a Record Magnetization Reversal Barrier over 1000 K, *J. Am. Chem. Soc.*, 2016, **138**, 5441; (*i*) C. Wang, R. Sun, Y. Chen, B.-W. Wang, Z.-M. Wang and S. Gao, Assembling High-Temperature Single-Molecule Magnets with Low-Coordinate Bis(amido) Dysprosium Unit $[DyN_2]^+$ via Cl-K-Cl Linkage, *CCS Chem.*, 2020, **2**, 362; (*j*) K.-X. Yu, J. G. C. Kragskow, Y.-S. Ding, Y.-Q. Zhai, D. Reta, N. F. Chilton and Y.-Z. Zheng, Enhancing Magnetic Hysteresis in Single-Molecule Magnets by Ligand Functionalization, *Chem*, 2020, **6**, 1777; (*k*) D. S. Krylov, F. Liu, S. M. Avdoshenko, L. Spree, B. Weise, A. Waske, A. U. B. Wolter, B. Büchner and A. A. Popov, Record-high thermal barrier of the relaxation of magnetization in the nitride clusterfullerene $Dy_2ScN@C_{80}$-I_h, *Chem. Commun.*, 2017, **53**, 7901; (*l*) S. Bala, G.-Z. Huang, Z.-Y. Ruan, S.-G. Wu, Y. Liu, L.-F. Wang, J.-L. Liu and M.-L. Tong, A square antiprism dysprosium single-ion magnet with an energy barrier over 900 K, *Chem. Commun.*, 2019, **55**, 9939; (*m*) M. Murrie, A. Canaj, S. Dey, E. Regincós Martí, C. Wilson and G. Rajaraman, Insight into D_{6h} Symmetry: Targeting Strong Axiality in Stable Dysprosium(III) Hexagonal Bipyramidal Single-Ion Magnets, *Angew. Chem., Int. Ed.*, 2019, **58**, 14146; (*n*) K. R. McClain, C. A. Gould, K. Chakarawet, S. Teat, T. J. Groshens, J. R. Long and B. G. Harvey, High-temperature magnetic blocking and magneto-structural correlations in a series of dysprosium (III) metallocenium single-molecule magnets, *Chem. Sci.*, 2018, **9**, 8492.

3 (*a*) A. Lunghi, F. Totti, R. Sessoli and S. Sanvito, The role of anharmonic phonons in under-barrier spin relaxation of single molecule magnets, *Nat. Commun.*, 2017, **8**, 14620; (*b*) L. Escalera-Moreno, J. J. Baldoví, A. Gaita-Ariño and E. Coronado, Spin states, vibrations and spin relaxation in molecular nanomagnets and spin qubits: a critical perspective, *Chem. Sci.*, 2018, **9**, 3265; (*c*) R. E. P. Winpenny, N. F. Chilton, M. Giansiracusa, D. Collison and A. Kostopoulos, Correlating Blocking Temperatures with Relaxation Mechanisms in Monometallic Single-Molecule Magnets with High Energy Barriers (U_{eff} > 600 K), *Chem. Commun.*, 2019, **55**, 7025; (*d*) C. A. P. Goodwin, F. Ortu, D. Reta, N. F. Chilton and D. P. Mills, Molecular magnetic hysteresis at 60 kelvin in dysprosocenium, *Nature*, 2017, **548**, 439; (*e*) A. Chiesa, F. Cugini, R. Hussain, E. Macaluso, G. Allodi, E. Garlatti, M. Giansiracusa, C. A. P. Goodwin, F. Ortu, D. Reta, J. M. Skelton, T. Guidi, *et al.*, Understanding magnetic relaxation in single-ion magnets with high blocking temperature, *Phys. Rev. B*, 2020, **101**, 174402.

4 (*a*) C. Y. Chow, H. Bolvin, V. E. Campbell, R. Guillot, J. W. Kampf, W. Wernsdorfer, F. Gendron, J. Autschbach, V. L. Pecoraro and T. Mallah, Assessing the exchange coupling in binuclear lanthanide(iii) complexes and the slow relaxation of the magnetization in the antiferromagnetically coupled Dy_2 derivative, *Chem. Sci.*, 2015, **6**, 4148; (*b*) Y.-N. Guo, G.-F. Xu, W. Wernsdorfer, L. Ungur, Y. Guo, J. Tang, H.-J. Zhang, L. F. Chibotaru and A. K. Powell, Strong Axiality and Ising Exchange Interaction Suppress Zero-Field Tunneling of Magnetization of an Asymmetric Dy2 Single-Molecule Magnet, *J. Am. Chem. Soc.*, 2011, **133**, 11948; (*c*) F. Habib and M. Murugesu, Lessons learned from dinuclear lanthanide nano-magnets, *Chem. Soc. Rev.*, 2013, **42**, 3278; (*d*) R. Westerström, J. Dreiser, C. Piamonteze, M. Muntwiler, S. Weyeneth, K. Krämer, S.-X. Liu, S. Decurtins, A. Popov, S. Yang, L. Dunsch and T. Greber, Tunneling, remanence, and frustration in dysprosium-based endohedral single-molecule magnets, *Phys. Rev. B: Condens. Matter Mater. Phys.*, 2014, **89**, 060406; (*e*) T. Han, M. J. Giansiracusa, Z.-H. Li, Y.-S. Ding, N. F. Chilton, R. E. P. Winpenny and Y.-Z. Zheng, Exchange-Biasing in a Dinuclear Dysprosium(III) Single-Molecule Magnet with a Large Energy Barrier for Magnetisation Reversal, *Chem. – Eur. J.*, 2020, **26**, 6773.

5 (*a*) S. Demir, I.-R. Jeon, J. R. Long and T. D. Harris, Radical ligand-containing single-molecule magnets, *Coord. Chem. Rev.*, 2015, **289–290**, 149; (*b*) S. Demir, M. I. Gonzalez, L. E. Darago, W. J. Evans and J. R. Long, Giant coercivity and high magnetic blocking temperatures for N_2^{3-} radical-bridged dilanthanide complexes upon ligand dissociation, *Nat. Commun.*, 2017, **8**, 2144; (*c*) F. Liu, G. Velkos, D. S. Krylov, L. Spree, M. Zalibera, R. Ray, N. A. Samoylova, C.-H. Chen, M. Rosenkranz, S. Schiemenz, F. Ziegs, K. Nenkov, *et al.*, Air-stable redox-active nanomagnets with lanthanide spins radical-bridged by a metal-metal bond, *Nat. Commun.*, 2019, **10**, 571.

6 (*a*) E. Moreno Pineda, N. F. Chilton, R. Marx, M. Dörfel, D. O. Sells, P. Neugebauer, S.-D. Jiang, D. Collison, J. van Slageren, E. J. L. McInnes and R. E. P. Winpenny, Direct measurement of dysprosium(III)$\cdots$dysprosium(III) interactions in a single-molecule magnet, *Nat. Commun.*, 2014, **5**, 5243; (*b*) M. J. Giansiracusa, E. Moreno-Pineda, R. Hussain, R. Marx, M. Martínez Prada, P. Neugebauer, S. Al-Badran, D. Collison, F. Tuna, J. van Slageren, S. Carretta, T. Guidi, *et al.*, Measurement of Magnetic Exchange in Asymmetric Lanthanide Dimetallics: Toward a

Transferable Theoretical Framework, *J. Am. Chem. Soc.*, 2018, **140**, 2504; (*c*) M. Gysler, F. El Hallak, L. Ungur, R. Marx, M. Hakl, P. Neugebauer, Y. Rechkemmer, Y. Lan, I. Sheikin, M. Orlita, C. E. Anson, A. K. Powell, *et al.*, Multitechnique investigation of Dy_3 – implications for coupled lanthanide clusters, *Chem. Sci.*, 2016, **7**, 4347; (*d*) R. T. Galeev, L. V. Mingalieva, A. A. Sukhanov, V. K. Voronkova, Y. Peng and A. K. Powell, Exchange Interactions in Heteronuclear Clusters Containing Dysprosium Ions: EPR Spectroscopy Possibility, *Appl. Magn. Reson.*, 2019, **50**, 1429.

7 (*a*) L. F. Chibotaru and N. Iwahara, Ising exchange interaction in lanthanides and actinides, *New J. Phys.*, 2015, **17**, 103028; (*b*) N. Iwahara and L. F. Chibotaru, New mechanism of kinetic exchange interaction induced by strong magnetic anisotropy, *Sci. Rep.*, 2016, **6**, 24743; (*c*) A. Palii, B. Tsukerblat, J. M. Clemente-Juan and E. Coronado, Magnetic exchange between metal ions with unquenched orbital angular momenta: basic concepts and relevance to molecular magnetism, *Int. Rev. Phys. Chem.*, 2010, **29**, 135; (*d*) A. Palii, B. Tsukerblat, S. Klokishner, K. R. Dunbar, J. M. Clemente-Juan and E. Coronado, Beyond the spin model: exchange coupling in molecular magnets with unquenched orbital angular momenta, *Chem. Soc. Rev.*, 2011, **40**, 3130; (*e*) N. Iwahara and L. F. Chibotaru, Exchange interaction between *J* multiplets, *Phys. Rev. B: Condens. Matter Mater. Phys.*, 2015, **91**, 174438.

8 (*a*) S. Yang, T. Wei and F. Jin, When metal clusters meet carbon cages: endohedral clusterfullerenes, *Chem. Soc. Rev.*, 2017, **46**, 5005; (*b*) A. A. Popov, S. Yang and L. Dunsch, Endohedral Fullerenes, *Chem. Rev.*, 2013, **113**, 5989.

9 (*a*) L. Spree and A. A. Popov, Recent advances in single molecule magnetism of dysprosium-metallofullerenes, *Dalton Trans.*, 2019, **48**, 2861; (*b*) C. Schlesier, L. Spree, A. Kostanyan, R. Westerström, A. Brandenburg, A. U. B. Wolter, S. Yang, T. Greber and A. A. Popov, Strong carbon cage influence on the single molecule magnetism in Dy–Sc nitride clusterfullerenes, *Chem. Commun.*, 2018, **54**, 9730; (*c*) C.-H. Chen, D. S. Krylov, S. M. Avdoshenko, F. Liu, L. Spree, R. Yadav, A. Alvertis, L. Hozoi, K. Nenkov, A. Kostanyan, T. Greber, A. U. B. Wolter, *et al.*, Selective arc-discharge synthesis of Dy_2S-clusterfullerenes and their isomer-dependent single molecule magnetism, *Chem. Sci.*, 2017, **8**, 6451; (*d*) K. Junghans, C. Schlesier, A. Kostanyan, N. A. Samoylova, Q. Deng, M. Rosenkranz, S. Schiemenz, R. Westerström, T. Greber, B. Büchner and A. A. Popov, Methane as a Selectivity Booster in the Arc-Discharge Synthesis of Endohedral Fullerenes: Selective Synthesis of the Single-Molecule Magnet $Dy_2TiC@C_{80}$ and Its Congener $Dy_2TiC_2@C_{80}$, *Angew. Chem., Int. Ed.*, 2015, **54**, 13411; (*e*) R. Westerström, J. Dreiser, C. Piamonteze, M. Muntwiler, S. Weyeneth, H. Brune, S. Rusponi, F. Nolting, A. Popov, S. Yang, L. Dunsch and T. Greber, An Endohedral Single-Molecule Magnet with Long Relaxation Times: $DySc_2N@C_{80}$, *J. Am. Chem. Soc.*, 2012, **134**, 9840; (*f*) D. Krylov, F. Liu, A. Brandenburg, L. Spree, V. Bon, S. Kaskel, A. Wolter, B. Buchner, S. Avdoshenko and A. A. Popov, Magnetization relaxation in the single-ion magnet $DySc_2N@C_{80}$: quantum tunneling, magnetic dilution, and unconventional temperature dependence, *Phys. Chem. Chem. Phys.*, 2018, **20**, 11656; (*g*) A. Brandenburg, D. S. Krylov, A. Beger, A. U. B. Wolter, B. Büchner and A. A. Popov, Carbide clusterfullerene $DyYTiC@C_{80}$ featuring three different metals in the endohedral cluster and its single-ion magnetism, *Chem. Commun.*, 2018, **54**, 10683; (*h*) L. Spree, C. Schlesier, A. Kostanyan, R. Westerström, T. Greber, B. Büchner, S. Avdoshenko and A. A. Popov, Single molecule magnets $DyM_2N@C_{80}$ and $Dy_2MN@C_{80}$ (M = Sc, Lu): The impact of diamagnetic metals on the Dy^{3+} magnetic anisotropy, Dy···Dy coupling, and mixing of molecular and lattice vibrations, *Chem. – Eur. J.*, 2020, **26**, 2436; (*i*) W. Yang, G. Velkos, F. Liu, S. M. Sudarkova, Y. Wang, J. Zhuang, H. Zhang, X. Li, X. Zhang, B. Büchner, S. M. Avdoshenko, A. A. Popov, *et al.*, Single Molecule Magnetism with Strong Magnetic Anisotropy and Enhanced Dy···Dy Coupling in Three Isomers of Dy-Oxide Clusterfullerene $Dy_2O@C_{82}$, *Adv. Sci.*, 2019, **6**, 1901352; (*j*) Y. Li, T. Wang, H. Meng, C. Zhao, M. Nie, L. Jiang and C. Wang, Controlling the magnetic properties of dysprosium metallofullerene within metal-organic framework, *Dalton Trans.*, 2016, **45**, 19226; (*k*) G. Velkos, W. Yang, Y.-R. Yao, S. M. Sudarkova, X. Liu, B. Büchner, S. M. Avdoshenko, N. Chen and A. A. Popov, Shape-adaptive single-molecule magnetism and hysteresis up to 14 K in oxide clusterfullerenes $Dy_2O@C_{72}$ and $Dy_2O@C_{74}$ with fused pentagon pairs and flexible Dy–(μ_2-O)–Dy angle, *Chem. Sci.*, 2020, **11**, 4766.

10 (*a*) G. Velkos, D. Krylov, K. Kirkpatrick, L. Spree, V. Dubrovin, B. Büchner, S. Avdoshenko, V. Bezmelnitsyn, S. Davis, P. Faust, J. Duchamp, H. Dorn, *et al.*, High blocking temperature of magnetization and giant coercivity in the azafullerene $Tb_2@C_{79}N$ with a single-electron Tb–Tb bond, *Angew. Chem., Int. Ed.*, 2019, **58**, 5891; (*b*) F. Liu, L. Spree, D. S. Krylov, G. Velkos, S. M. Avdoshenko and A. A. Popov, Single-Electron Lanthanide-Lanthanide Bonds Inside Fullerenes toward Robust Redox-Active Molecular Magnets, *Acc. Chem. Res.*, 2019, **52**, 2981; (*c*) F. Liu, D. S. Krylov, L. Spree, S. M. Avdoshenko, N. A. Samoylova, M. Rosenkranz, A. Kostanyan, T. Greber, A. U. B. Wolter, B. Büchner and A. A. Popov, Single molecule magnet with an unpaired electron trapped between two lanthanide ions inside a fullerene, *Nat. Commun.*, 2017, **8**, 16098; (*d*) Y. Wang, J. Xiong, J. Su, Z.-Q. Hu, F. Ma, R. Sun, X.-Y. Tan, H.-L. Sun, B. Wang, Z. Shi and S. Gao, $Dy_2@C_{79}N$: A New Member of Dimetalloazafullerenes with Strong Single Molecular Magnetism, *Nanoscale*, 2020, **12**, 11130.

11 (*a*) S.-Y. Lin, W. Wernsdorfer, L. Ungur, A. K. Powell, Y.-N. Guo, J. Tang, L. Zhao, L. F. Chibotaru and H.-J. Zhang, Coupling Dy_3 Triangles to Maximize the Toroidal Moment, *Angew. Chem., Int. Ed.*, 2012, **51**, 12767; (*b*) Y.-X. Wang, W. Shi, H. Li, Y. Song, L. Fang, Y. Lan,

A. K. Powell, W. Wernsdorfer, L. Ungur, L. F. Chibotaru, M. Shen and P. Cheng, A single-molecule magnet assembly exhibiting a dielectric transition at 470 K, *Chem. Sci.*, 2012, **3**, 3366.

12 A. Kostanyan, R. Westerström, D. Kunhardt, B. Büchner, A. A. Popov and T. Greber, Sub-Kelvin hysteresis of the dilanthanide single-molecule magnet $Tb_2ScN@C_{80}$, *Phys. Rev. B*, 2020, **101**, 134429.

13 (*a*) J. Hafner, *Ab initio* simulations of materials using VASP: Density-functional theory and beyond, *J. Comput. Chem.*, 2008, **29**, 2044; (*b*) G. Kresse and J. Hafner, Ab initio molecular dynamics for liquid metals, *Phys. Rev. B: Condens. Matter Mater. Phys.*, 1993, **47**, 558; (*c*) G. Kresse and D. Joubert, From ultrasoft pseudopotentials to the projector augmented-wave method, *Phys. Rev. B: Condens. Matter Mater. Phys.*, 1999, **59**, 1758; (*d*) J. P. Perdew, K. Burke and M. Ernzerhof, Generalized gradient approximation made simple, *Phys. Rev. Lett.*, 1996, **77**, 3865; (*e*) S. Grimme, Density functional theory with London dispersion corrections, *Wiley Interdiscip. Rev.: Comput. Mol. Sci.*, 2011, **1**, 211.

14 N. F. Chilton, R. P. Anderson, L. D. Turner, A. Soncini and K. S. Murray, PHI: A powerful new program for the analysis of anisotropic monomeric and exchange-coupled polynuclear d- and f-block complexes, *J. Comput. Chem.*, 2013, **34**, 1164.

15 (*a*) X. Yi, K. Bernot, F. Pointillart, G. Poneti, G. Calvez, C. Daiguebonne, O. Guillou and R. Sessoli, A Luminescent and Sublimable Dy^{III}-Based Single-Molecule Magnet, *Chem. – Eur. J.*, 2012, **18**, 11379; (*b*) J. Xiong, H.-Y. Ding, Y.-S. Meng, C. Gao, X.-J. Zhang, Z.-S. Meng, Y.-Q. Zhang, W. Shi, B.-W. Wang and S. Gao, Hydroxide-bridged five-coordinate Dy^{III} single-molecule magnet exhibiting the record thermal relaxation barrier of magnetization among lanthanide-only dimers, *Chem. Sci.*, 2017, **8**, 1288; (*c*) G. Huang, X. Yi, J. Jung, O. Guillou, O. Cador, F. Pointillart, B. Le Guennic and K. Bernot, Optimization of Magnetic Relaxation and Isotopic Enrichment in Dimeric Dy^{III} Single-Molecule Magnets, *Eur. J. Inorg. Chem.*, 2018, **2018**, 326.

16 K. N. Shrivastava, Theory of Spin–Lattice Relaxation, *Phys. Status Solidi B*, 1983, **117**, 437.

17 F. Tuna, C. A. Smith, M. Bodensteiner, L. Ungur, L. F. Chibotaru, E. J. L. McInnes, R. E. P. Winpenny, D. Collison and R. A. Layfield, A High Anisotropy Barrier in a Sulfur-Bridged Organodysprosium Single-Molecule Magnet, *Angew. Chem., Int. Ed.*, 2012, **51**, 6976.

18 W. Zhang, S.-M. Xu, Z.-X. Zhu, J. Ru, Y.-Q. Zhang and M.-X. Yao, Strong intramolecular Dy^{III}–Dy^{III} magnetic couplings up to 15.00 cm^{-1} in phenoxyl-bridged dinuclear 4f complexes, *New J. Chem.*, 2020, **44**, 2083.

19 X.-Q. Ji, F. Ma, J. Xiong, J. Yang, H.-L. Sun, Y.-Q. Zhang and S. Gao, A rare chloride-bridged dysprosium chain with slow magnetic relaxation: a thermally activated mechanism via a second-excited state promoted by magnetic interactions, *Inorg. Chem. Front.*, 2019, **6**, 786.

20 S. Xue, Y.-N. Guo, L. Ungur, J. Tang and L. F. Chibotaru, Tuning the Magnetic Interactions and Relaxation Dynamics of Dy_2 Single-Molecule Magnets, *Chem. – Eur. J.*, 2015, **21**, 14099.

21 L. Ungur, M. Thewissen, J.-P. Costes, W. Wernsdorfer and L. F. Chibotaru, Interplay of Strongly Anisotropic Metal Ions in Magnetic Blocking of Complexes, *Inorg. Chem.*, 2013, **52**, 6328.

22 M. E. Lines, Orbital Angular Momentum in the Theory of Paramagnetic Clusters, *J. Chem. Phys.*, 1971, **55**, 2977.

23 D. N. Woodruff, F. Tuna, M. Bodensteiner, R. E. P. Winpenny and R. A. Layfield, Single-Molecule Magnetism in Tetrametallic Terbium and Dysprosium Thiolate Cages, *Organometallics*, 2013, **32**, 1224.

24 (*a*) M. A. Ruderman and C. Kittel, Indirect Exchange Coupling of Nuclear Magnetic Moments by Conduction Electrons, *Phys. Rev.*, 1954, **96**, 99; (*b*) T. Kasuya, A Theory of Metallic Ferro- and Antiferromagnetism on Zener's Model, *Prog. Theor. Phys.*, 1956, **16**, 45; (*c*) K. Yosida, Magnetic Properties of Cu-Mn Alloys, *Phys. Rev.*, 1957, **106**, 893.

25 (*a*) S. R. Power and M. S. Ferreira, Indirect Exchange and Ruderman–Kittel–Kasuya–Yosida (RKKY) Interactions in Magnetically-Doped Graphene, *Crystals*, 2013, **3**, 49; (*b*) K. Szałowski, RKKY coupling between impurity spins in graphene nanoflakes, *Phys. Rev. B: Condens. Matter Mater. Phys.*, 2011, **84**, 205409; (*c*) J. Klinovaja and D. Loss, RKKY interaction in carbon nanotubes and graphene nanoribbons, *Phys. Rev. B: Condens. Matter Mater. Phys.*, 2013, **87**, 045422.

26 (*a*) F. Neese, Software update: the ORCA program system, version 4.0, *Wiley Interdiscip. Rev.: Comput. Mol. Sci.*, 2018, **8**, e1327; (*b*) F. Neese, The ORCA program system, *Wiley Interdiscip. Rev.: Comput. Mol. Sci.*, 2012, **2**, 73; (*c*) F. Neese, F. Wennmohs, A. Hansen and U. Becker, Efficient, approximate and parallel Hartree-Fock and hybrid DFT calculations. A 'chain-of-spheres' algorithm for the Hartree-Fock exchange, *Chem. Phys.*, 2009, **356**, 98.

27 (*a*) D. A. Pantazis and F. Neese, All-Electron Scalar Relativistic Basis Sets for the Lanthanides, *J. Chem. Theory Comput.*, 2009, **5**, 2229; (*b*) D. A. Pantazis, X.-Y. Chen, C. R. Landis and F. Neese, All-Electron Scalar Relativistic Basis Sets for Third-Row Transition Metal Atoms, *J. Chem. Theory Comput.*, 2008, **4**, 908.

28 W. Humphrey, A. Dalke and K. Schulten, VMD - Visual Molecular Dynamics, *J. Mol. Graphics*, 1996, **14**, 33.

